Pressure Induced Orientational Ordering in *p*-Terphenyl

N. Arul Murugan and S. Yashonath*

Solid State and Structural Chemistry Unit, Indian Institute of Science, Bangalore 560 012, India

Received: September 10, 2004; In Final Form: October 27, 2004

Three different interaction potentials existing in the literature along with a model proposed here have been used to model *p*-terphenyl under standard conditions. Of these, the model that predicts the room-temperature crystal structure well has been used to understand the behavior of *p*-terphenyl under pressure. Lattice parameters show good agreement with the X-ray diffraction values reported by Puschnig et al. (Puschnig, P.; Heimel, G.; Weinmeier, K.; Resel, R.; Ambrosch-Draxl, C. *High Pressure Res.* **2002**, *22*, 105). The nonplanar structure of *p*-terphenyl transforms to a planar structure with gradual disappearance of disorder associated with ring flipping. We show that the transformation is accompanied by a change in the potential energy profile from W-shaped to a U-shaped form, which is associated with complete planarization between 1.0 and 1.5 GPa. Our results reported here are in excellent agreement with X-ray diffraction results which also suggest the existence of a similar transition as a function of pressure in polyphenyls such as biphenyl and *p*-hexaphenyl. Interestingly, the amplitude of the torsional motion is largest at an intermediate pressure of 1.0 GPa. This is attributed to the rather flat potential energy landscape which occurs during the transition from W- to U-shaped potential.

1. Introduction

In the search for low-cost, easy-to-process materials for electrooptic and electronic applications, materials such as polyacetylene and π-conjugated materials have attracted considerable attention. For this, an understanding of the properties of polyphenyls at both microscopic and macroscopic levels is important.

Baudour et al.[1,2] have reported the crystal structure of low-temperature (113 K) *p*-terphenyl. The space group is $P\bar{1}$ ($Z = 4$) with no disorder. With increase in temperature, this phase transforms at 193 K to a monoclinic phase, $P2_1/a$ ($Z = 2$). The librational amplitude of the central ring changes from $\langle\theta^2\rangle = 19.3$ deg^2 at 113 K to $\langle\theta^2\rangle = 260.3$ deg^2 at room temperature.[3] This temperature-induced order−disorder transition has been observed for a range of polyphenyls starting from biphenyl to *p*-hexaphenyl.[4,5]

Heimel et al.[6] report the pressure-induced structural changes in polyphenyls, starting with biphenyl and up to *p*-hexaphenyl using X-ray powder diffraction experiments. They discuss the implication of changes in intermolecular distances (due to molecular rearrangement) on the bulk properties such as optical response and charge transport. Puschnig et al.[7] report structural details of *p*-terphenyl as a function of pressure from X-ray diffraction measurements. Further, they have carried out ab initio band structure calculations using the experimental structure as a function of pressure. They report the effect of changes in the distance between the molecules and their orientation on the optical response of the material.

There have been several computational studies on polyphenyls. Baranyai et al.[8] carried out molecular dynamics calculations on polyphenyls above and below the transition temperature. Specifically, they investigate the role of the torsional potential in determining the conformation of the molecule in the solid state. They observe a bimodal distribution of dihedral angles when the torsional forces are large. When these forces are decreased, unimodal distribution is seen. The conformation of the molecules in the solid state is decided by two different interactions, namely, intermolecular interactions and inter-ring torsional potential. The intermolecular interactions always favor planar conformation for molecules as it results in effective packing. On the other hand, the torsional interaction of the BHS form favors a twisted form (BHS = Benkert, Heine and Simmons). So, when the torsional barrier is low, the molecules prefer to be in planar form.

In general, whenever classical potentials are employed in simulations, it may often be necessary to use different model potentials over different regions of pressure. At low pressures, the region of the potential function close to the minimum is sampled most frequently. With increase in pressure, the intermolecular interactions at shorter distances are sampled more frequently as a result of a decrease in the distance between the neighboring molecules. In this case, the repulsive portion of the potential function becomes important. This may necessitate the use of a different potential function in many cases, especially if the simulations are carried out at extremely high pressures.

Recently, Bordat et al.[9] carried out molecular dynamics calculations using the modified inter-ring torsional potential of Tsuzuki and Tanabe.[10] They have studied the system at different temperatures and characterized the system using structural quantities such as dihedral angle distributions of the two torsional angles. They also report a probability density $f(\phi_1, \phi_2)$ as well as dynamical properties such as auto- and cross-correlation function for inter-ring torsions.

Here, we study the *p*-terphenyl as a function of pressure. *p*-Terphenyl at room temperature and 1 atm pressure has been modeled using four different intermolecular and inter-ring torsional potentials. A detailed pressure-dependent study has been carried out using the potentials that best describe the room-temperature crystal structure of *p*-terphenyl, namely, the modified Filippini intermolecular potential and BHS intramolecular potential. The high-pressure phase has been characterized by various structural quantities such as radial distribution functions,

10.1021/jp045913k CCC: $30.25
Published on Web 01/08/2005

TABLE 1: Intermolecular (D. E. Williams) and Intramolecular Potential Parameters (BHS) (Model I)

type	b_{ij}, kJ/mol	c_{ij}, Å^{-1}	a_{ij}, kJ/mol Å^6
C−C	369 743.0	3.60	2439.8
C−H	66 529.6	3.67	576.8
H−H	11 971.0	3.74	136.4

charges, q/e

C	−0.153
H	0.153

BHS Potential

g	L, kJ/mol	M, kJ/mol	N, rad^{-2}
2	35.2	41.05	2.52

TABLE 2: Intermolecular (Gavezzotti and Filippini) and Intramolecular Potential (BHS) Parameters (Model II)

type	b_{ij}, kJ/mol	c_{ij}, Å^{-1}	a_{ij}, kJ/mol Å^6
C−C	226 145.0	3.47	2418.0
C−H	120 792.0	4.10	473.0
H−H	24 158.0	4.01	109.2

charges, q/e

C	0.00
H	0.00

BHS Potential

g	L, kJ/mol	M, kJ/mol	N, rad^{-2}
2	35.2	41.05	2.52

average cell parameters, dihedral angles, and contour plot of ϕ_1 and ϕ_2. The cell parameters are compared with the lattice parameters obtained from X-ray diffraction by Puschnig et al.[7] It is seen that the disordered structure undergoes a transformation to a well-ordered phase between 1.0 and 1.5 GPa.

2. Potential Functions and Monte Carlo Method

2.1. Intermolecular Potential. Four different intermolecular potential models have been employed for simulating the room-temperature (300 K) phase of *p*-terphenyl at 1 atm pressure. They are the potential models of Williams,[11] Filippini and Gavezzotti,[12] and Bordat and Brown[9] and the Filippini potential after suitable modification. The form of the potential function in all cases is of Buckingham 6-exp form with an additional Coulombic term (see eq 1). The Coulombic term is included only in cases of models by Williams and by Bordat and Brown. Williams potential parameters have been derived by fitting to about 30 aromatic and nonaromatic hydrocarbons. The Williams[11] potential places a charge of $+q$ ($q = 0.153|e|$) on each hydrogen and a charge of $-q$ on each carbon atom. The potential parameters are listed in Table 1.

$$u_{ij}(r_{ij}) = b_{ij}\exp(-r_{ij}c_{ij}) - a_{ij}/r_{ij}^{\,6} + q_iq_j/r_{ij} \qquad (1)$$

The potential parameters by Filippini and Gavezzotti (FG)[12] are based on the distribution of atom−atom distances in 1846 organic crystals, structural data of 217 organic crystals, and the heats of sublimation of 122 compounds. Although no electrostatic interaction is included explicitly in the FG potential, they[12] suggest that it is included implicitly by the use of effective potential parameters which lead to an additional lowering of the well-depth of the (6-exp) potential for cross or unlike interactions. The potential parameters are listed in Table 2. The potential parameters of Brown and Bordat[9] were derived by optimizing the parameters of Williams[13] (optimized for aliphatic hydrocarbons) to obtain better agreement of calculated lattice parameters with the experimentally derived values.[14] These parameters are listed in Table 3. The modified Filippini parameters are based on the parameters originally proposed by Filippini and Gavezzotti[12] but modified by us for *p*-terphenyl by minimizing the forces acting on the molecules to ensure better agreement with the experimental lattice parameters. The parameters are listed in Table 4.

TABLE 3: Intermolecular (Bordat and Brown) and Intramolecular Potential Parameters (Model III)

type	b_{ij}, kJ/mol	c_{ij}, Å^{-1}	a_{ij}, kJ/mol Å^6
C−C	85 774 050.0	6.02	1493.7
C−H	1 540 173.8	4.95	335.4
H−H	27 656.2	3.87	75.3

charges, q/e

1	−0.130
2	−0.200
3	−0.180
4	0.080
5	−0.080
6	−0.155
7	0.160
8	0.170
9	0.180
10	0.170

AM1 Model 1

A_2, kJ/mol	A_4, kJ/mol	A_6, kJ/mol	A_8, kJ/mol
0.502 1	1.577 4	0.543 9	0.127 6

TABLE 4: Intermolecular (Modified Gavezzotti and Filippini) and Intramolecular Potential (BHS) Parameters (Model IV)

type	b_{ij}, kJ/mol	c_{ij}, Å^{-1}	a_{ij}, kJ/mol Å^6
C−C	130 535.1	3.47	2 301.1
C−H	111 536.1	4.10	584.2
H−H	27 932.4	4.01	63.3

charges, q/e

C	0.00
H	0.00

BHS Potential

g	L, kJ/mol	M, kJ/mol	N, rad^{-2}
2	35.2	41.05	2.52

2.2. Intramolecular Potential. Two different intramolecular potential functions have been used to include the inter-ring twist motion of phenyl rings in *p*-terphenyl. The first model is by Benkert, Heine, and Simmons (BHS).[15] The potential function has the following form:

$$u(\phi) = g[L\exp(-N\phi^2) + M\sin^2(\phi)] \qquad (2)$$

The parameters are listed in Table 1. This potential includes two contributions: conjugation energy which stabilizes the planar form and repulsion term which stabilizes the twisted form.

The other model is based on the torsional potential of biphenyl determined by the Austin model 1 (AM1), semiempirical Hamiltonian at the restricted Hartree−Fock level, and modified by Bordat and Brown.[9] The potential function is of the following form:

$$u(\phi) = A_2(1+\cos(2\phi)) + A_4(1+\cos(4\phi)) + A_6(1+\cos(6\phi)) + A_8(1+\cos(8\phi)) \qquad (3)$$

The coefficients are listed in Table 3.

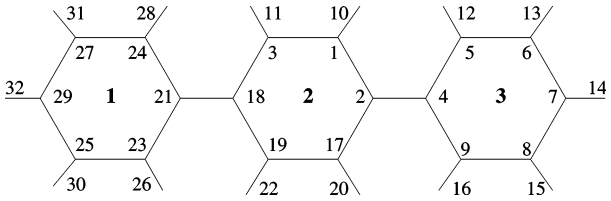

Figure 1. Molecular structure and numbering of *p*-terphenyl.

We have carried out isothermal−isobaric Monte Carlo (NPT-MC) calculations with variable shape simulation cell for four different models in order to see which of these provide a description closest to experimental structure. Toward this, we have carried out calculations with (i) Williams potential for intermolecular interactions along with BHS potential for torsional motion (model I), (ii) Filippini potential with BHS (model II), (iii) modified Williams with AM1 for intramolecular (torsional) potential used previously by Bordat and Brown[9] (model III), and finally, (iv) modified Filippini and Gavezzotti with BHS for intramolecular interactions (model IV).

2.3. Variable Shape NPT-MC Simulations. Simulations have been carried out in isothermal−isobaric or NPT ensemble with variable shape simulation[16] cell using the Monte Carlo method and the importance sampling algorithm of Metropolis.[17] The simulation cell is represented by 9 degrees of freedom. In addition, each molecule has 8 degrees of freedom: three translational, three rotational, and two torsional associated with the two dihedral angles, ϕ_1(between the two phenyl rings 1 and 2) and ϕ_2 (between the other two phenyl rings 2 and 3, see Figure 1). Thus, the average of any property $a(\mathbf{r}^N, \Omega^N, \phi_1{}^N, \phi_2{}^N, \mathbf{a}, \mathbf{b}, \mathbf{c})$ is obtained by integrating over these $(8N + 9)$ variables:

$$\langle a\rangle = [\int d\mathbf{a} \int d\mathbf{b} \int d\mathbf{c} \int d\Omega^N \int d\phi_1^N \int d\phi_2^N \int d\mathbf{r}^N \; a(\mathbf{r}^N, \Omega^N, \phi_1^N, \phi_2^N) p(\mathbf{r}^N, \Omega^N, \phi_1^N, \phi_2^N)]/ [\int d\mathbf{a} \int d\mathbf{b} \int d\mathbf{c} \int d\Omega^N \int d\phi_1^N \int d\phi_2^N \int d\mathbf{r}^N \; p(\mathbf{r}^N, \Omega^N, \phi_1^N, \phi_2^N)] \quad (4)$$

where $p(\mathbf{r}^N, \Omega^N, \phi_1^N, \phi_2^N) = e^{-\beta U(\mathbf{r}^N, \Omega^N, \phi_1{}^N, \phi_2{}^N)}$ and $a(\mathbf{r}^N, \Omega^N, \phi_1^N, \phi_2^N)$ are the probability and the property, respectively for each configuration specified by $(\mathbf{r}^N, \Omega^N, \phi_1^N, \phi_2^N)$. Here $\mathbf{r}^N$'s are the center of mass positions of the molecules, and Ω^N's specify the orientations of molecules as a whole, while ϕ_1^N and ϕ_2^N specify the dihedral angles of the N molecular species. Note that $\mathbf{r}$ and Ω have three components each: $\mathbf{r}$ specifies the three Cartesian coordinates and Ω the three Euler angles. Variable shape simulation cell was employed as it provides the necessary degrees of freedom for the simulation cell to be in any one of the crystal systems. The simulation cell is represented by three vectors, the cell vectors, **a**, **b**, and **c**. Parrinello and Rahman[16] originally chose the three vectors without any constraints. The cell vectors contribute 9 additional degrees of freedom. However, as Yashonath and Rao[18] showed subsequently, only 6 degrees of freedom are necessary for representing the simulation cell. These could be, for example, the typical cell parameters a, b, c, α, β, and γ. The 3 additional degrees of freedom in the original formulation of Parrinello and Rahman[16] often leads to rotation of the simulation cell[18] as a whole especially in polyatomic systems which is not desirable. This can be overcome by reducing the 9 degrees of freedom to the essential six. This has been accomplished here by choosing vector **a** along x-axis, **b** in xy-plane, and **c** in any direction.[18] This leads to a total of 6 degrees of freedom. This permits the system to undergo solid−solid phase transformation from one space group to another. Thus, the simulation involves integration over $(8N + 6)$ degrees of freedom only. Martyna et al.[19] provide a more detailed discussion on the alternative methods of preventing cell rotation in an isothermal−isobaric ensemble simulation using the molecular dynamics method. In systems such as biphenyl,[20] stilbene, or *p*-terphenyl, the amplitude of atomic displacement due to torsional mode is comparable to the atomic displacement due to molecular translation or rotation modes. Hence, it is necessary to sample over the torsional degrees of freedom in the configurational phase space.

3. Computational Details

The starting configuration for the simulation is taken as the X-ray structure at 200 K provided by Baudour et al.[21] The first set of runs simulate *p*-terphenyl at 300 K and 1 atm pressure by employing the four different potential models described previously. The purpose of these calculations is to choose the best potential for study of the effect of pressure on the structure of *p*-terphenyl.

The second set of calculations vary the pressure and study its effect on structure and dynamics. On the basis of the first set of MC runs, it was found that the modified Filippini and Gavezzotti with BHS model (model IV) provided a better description of the room-temperature structure of *p*-terphenyl. Therefore, we choose this potential for these sets of runs as their results are likely to be most reliable. We have employed a temperature of 300 K but varied the pressure from 1 atm to 4.0 GPa in steps of 0.5 GPa. Finally, a run at 5.0 GPa has been carried out.

For all these simulations, the initial configuration is taken from the final configuration of the previous low-pressure run. Simulations have been performed on $5 \times 7 \times 3$ unit cells of *p*-terphenyl. Simulations have been carried out for 25 000 MC steps including 5000 for equilibration. The center of mass (com)−com cutoff employed for all the simulations in both sets is 13 Å. Direct summation of charges over spheres that are neutral is employed whenever Coulomb interactions are present. Since the magnitude of the charge on the atoms is small, this is adequate. In models where the electrostatic contribution is significant, Ewald summation will be required.

4. Results and Discussion

4.1. Structure of Room-Temperature Phase. As the room-temperature crystal structure and lattice parameters of *p*-terphenyl are known, we use this as a benchmark to distinguish between the four models. Table 5 lists the average lattice parameters predicted by the four potential models along with the values obtained from X-ray diffraction. Percentage deviation of the lattice parameters from these experimental values is listed in parentheses. Note that the deviations in almost all lattice parameters except the deviation of the c parameter is within 7%. Models I and II, both yield significantly large deviation for c (21.4 and 15.5%). We therefore exclude use of these models for simulations involving pressure variation. Between models III and IV, model III shows a better agreement of b but poorer agreement of c. However, if we look at the sum of the squares of the deviations,

$$s = \frac{1}{6}\sum_{i=1}^{6}(\alpha_i - \alpha_{i,\mathrm{ex}})^2 \quad (5)$$

where α_i and $\alpha_{i,\mathrm{ex}}$ stand for the simulated and experimental lattice parameters, respectively, the values for models III and

TABLE 5: Average Cell Parameters (with the Percentage Deviation) at 300 K for Models I−IV Compared with the Experimental Cell Parameters

	a, Å	*b*, Å	*c*, Å	α, deg	*β*, deg	*γ*, deg
XRD	8.02	5.58	13.58	90.00	92.10	90.00
model I	8.52 (6.2)	5.47 (−2.0)	16.49 (21.4)	86.67 (−3.7)	91.04 (−1.2)	89.91 (−0.1)
model II	8.30 (3.5)	5.40 (−3.2)	15.68 (15.5)	91.14 (1.3)	88.85 (−3.5)	89.97 (−0.0)
model III	7.83 (−2.4)	5.77 (3.4)	12.15 (−10.5)	91.25 (1.4)	97.26 (5.6)	89.38 (−0.7)
model IV	8.11 (1.1)	5.21 (−6.6)	12.73 (−6.3)	88.94 (−1.2)	90.42 (−1.8)	89.87 (−0.1)

IV are 26.90 and 14.86, respectively. Clearly, model IV is the best. Further calculations have been carried out with model IV.

4.2. Pressure Induced Orientational Ordering. The variation of cell parameters as a function of pressure between 0 and 5.0 GPa is shown in Figure 2. The simulated cell parameters

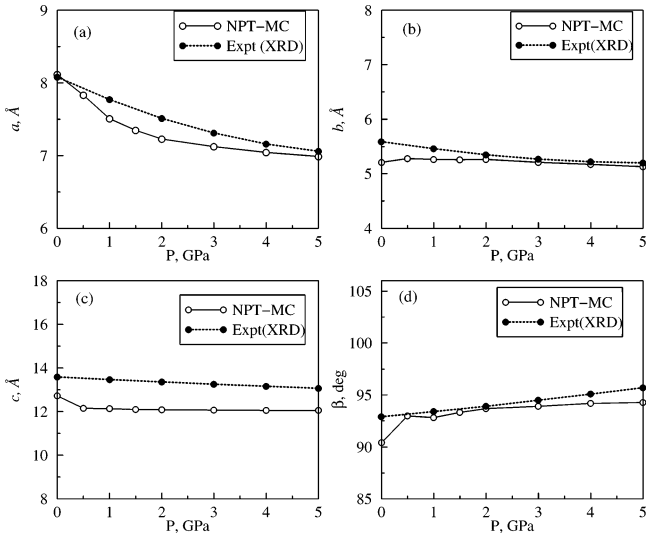

Figure 2. Variation of cell parameters (both simulated and experimental) as a function of pressure: (a) *a*, (b) *b*, (c) *c*, (d) *β*.

are compared to the cell parameters from X-ray diffraction studies by Puschnig et al.[7] as a function of pressure. The trends in the cell parameters with increase in pressure are well reproduced by the isothermal−isobaric simulations. In fact the deviations of the *b* parameter show significant decrease at higher pressures. The deviation of 7% in *c* persists even at higher pressures. As Hsu and Williams[22] point out, these are within the acceptable thresholds. In their extensive studies, they have found that if three out of the six parameters are within the threshold, the potential is acceptable.

We have also computed the magnitude of statistical fluctuation or variance in the cell parameters *a*, *b*, and *c* from

$$\sigma^2 = \langle A^2 \rangle - \langle A \rangle \langle A \rangle \qquad (6)$$

The calculated average over 20 000 MC steps gave 0.166, 0.177, and 0.005 for *a*, *b*, and *c*, respectively. The variance in *a* and *b* is significantly larger than the variance in *c*. Figure 3 shows one unit cell of *p*-terphenyl obtained from the X-ray crystal structure of Baudour et al.[21] along with the crystallographic axes. It is evident from this that the molecular axis of *p*-terphenyl is nearly parallel to the *c*-axis. Any torsional motion of the phenyl rings leads to large fluctuations along the *a*-axis and *b*-axis. Such torsional motion, however, does not lead to significant changes in the *c*-axis. This is responsible for the large fluctuation in the *a*- and *b*-axis seen in the simulation.

Figure 4 shows the variation of unit cell volume compared to the experimental unit cell volume. Even though the trend is well-produced, the calculated volume is lower by about 10% over the whole range of pressure. Figure 5 shows the center of mass (com)−com, C−C, C−H, and H−H radial distribution functions (rdf's) as a function of pressure. At 1 atm pressure and 300 K, the C−C, C−H, and H−H rdf's do not show any well-defined peaks suggesting the presence of a significant

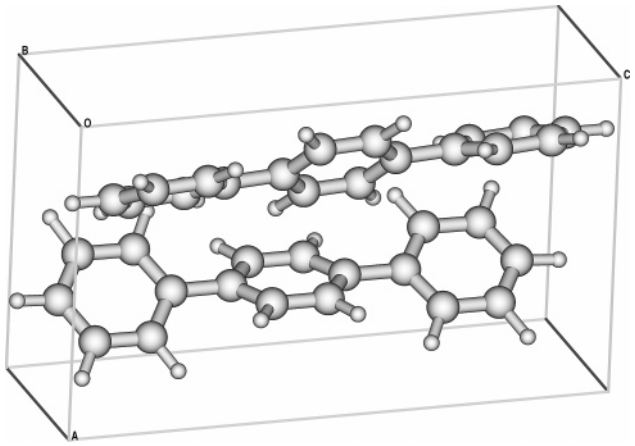

Figure 3. Unit cell of *p*-terphenyl[20] along with crystallographic axes.

degree of disorder. With increase in pressures, C−C, C−H, and H−H rdf's begin to develop significant structure and well-defined peaks appear indicating possible ordering of the system. The appearance of new peaks in the com−com rdf suggests that ordering also alters the translational ordering in the lattice.

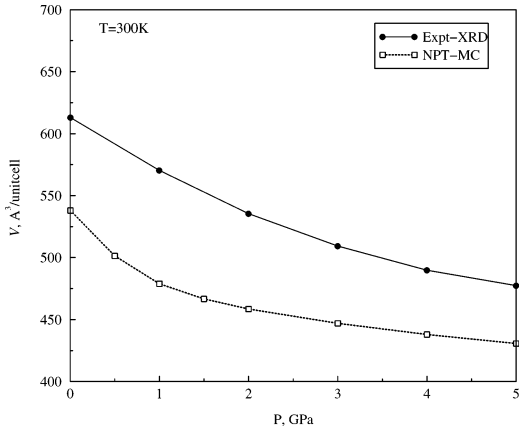

Figure 4. Variation of unit cell volume *V* (both simulated and experimental) as a function of pressure.

These changes are seen to occur up to a pressure of 1.0 GPa. Beyond 1.0 GPa, little or no changes in the rdf are seen. This is also reflected in the variation of lattice parameters shown in Figure 2 where the changes are limited largely to 0.0−1.0 GPa. The well-defined peaks in the com−com rdf suggest that the molecules are translationally ordered. The nature of disorder has been discussed by a number of groups in the literature.[1−3]

Parts a and b of Figure 6 show the snapshots of molecules at pressures 1 atm and 5 GPa, respectively, at a temperature of 300 K. The view is along the *c*-axis. It is clear from the figures that almost all the molecules are with twisted conformation at

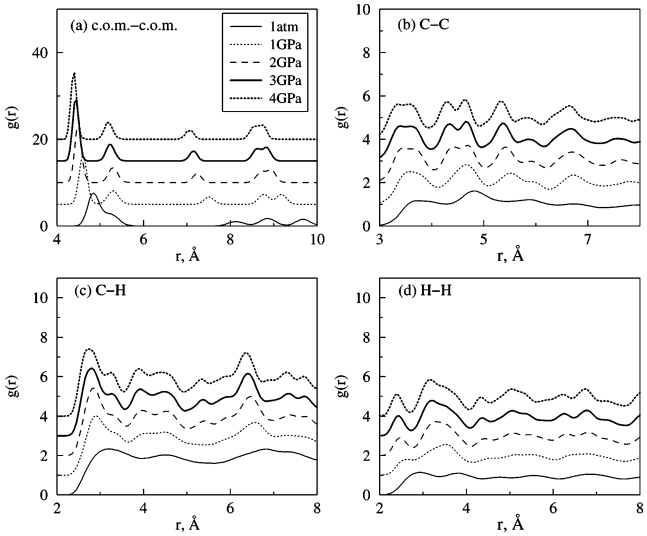

Figure 5. The com−com, C−C, C−H, and H−H pair correlation functions as a function of pressure.

1 atm and 300 K. It is also evident that the high-pressure phase is fully orientationally ordered and all the molecules are planar. Parts c and d of Figure 6 again show the snapshots of molecules at two different pressures of 1 atm and 5.0 GPa, respectively, at a temperature of 300 K. Here, the view is along the *b*-axis of the lattice. From parts c and d of Figure 6, it is clear that the interlayer distance along the *c* direction is considerably reduced when the pressure is increased from 1 atm to 5 GPa. This can be partly attributed to the shift toward higher *r* of the second peak in the com−com rdf and shift toward lower *r* of the third peak. Parts e and f of Figure 6 show the snapshots of molecules at two different pressures of 1 atm and 5.0 GPa, respectively, at a temperature of 300 K. Here, the view is along the long molecular axis.

Figure 7 shows the variation of U_{inter}, U_{intra}, and U_{total} as a function of pressure. The intermolecular energy, U_{inter}, defined as

$$U_{\text{inter}} = \frac{1}{2N}\sum_{a=1}^{N}\sum_{b=1}^{N}\sum_{i=1}^{N_s}\sum_{j=1}^{N_s} u_{ij}(r_{ij,ab}) \tag{7}$$

where *a* and *b* refer to the molecules and *i* and *j* refer to the interaction sites placed at the positions of C and H. Here, N_s (=32) is the number of sites on *p*-terphenyl and $N = 210$. u_{ij} is given by the expression in eq 1. The intramolecular energy U_{intra} and U_{total} are given by

$$U_{\text{intra}} = \frac{1}{N}\sum_{i=1}^{N}(u_i(\phi_{i,1}) + u_i(\phi_{i,2})) \tag{8}$$

$$U_{\text{total}} = U_{\text{inter}} + U_{\text{intra}} \tag{9}$$

U_{inter} shows a minimum at 1.5 GPa. An increase in pressure results in better packing and hence stronger molecular interactions. But as the pressure increases still further, molecules come closer resulting in repulsion from neighboring molecules. U_{intra} shows a steady increase up to 2.0 GPa. At still higher pressures, it reaches a constant value, indicating that conformational changes occurring in the molecular level have attained a saturation at this pressure. As a result of competition between intermolecular and intramolecular energies, the variation of U_{total} shows a minimum at 0.5 GPa.

Figure 8 shows the variation of average dihedral angle and average absolute dihedral angle as a function of pressure. The averaging has been carried out over both the dihedral angles ϕ_1 and ϕ_2 as they are equivalent. It is clear that the average dihedral angle remains zero indicating the average structure to be planar at all pressures studied here. But the average absolute dihedral angle $|\phi|$ has nonzero magnitude indicating that at any given instant phenyl rings are nonplanar. In other words, the most probable distribution is at $\phi = 0°$. With increase in pressure, $|\phi|$ decreases and reaches a constant value beyond 2.0 GPa, indicating the molecular conformation is no longer altered after 2.0 GPa.

Figure 9 shows the distributions of dihedral angles $f(\phi)$, $f(\phi_1)$, $f(\phi_2)$, and $f(\phi_3)$ (ϕ_3 is the dihedral angle between the phenyl rings 1 and 3). $f(\phi)$ obtained by averaging over the dihedral angles ϕ_1 and ϕ_2 is shown in Figure 9 along with individual distributions $f(\phi_1)$, $f(\phi_2)$, and $f(\phi_3)$. It is evident from the distributions that at higher pressures the molecules become planar. The fact that $f(\phi_3)$ has an unimodal distribution with a maximum around $\phi_3 = 0°$ suggests the motion of rings 1 and 3 occurs in phase.

Note that the distributions $f(\phi_1)$ and $f(\phi_2)$ are asymmetric with respect to $\phi_1 = 0°$. $f(\phi_1)$ ($f(\phi_2)$) has a larger population for $\phi > 0°$ ($\phi < 0°$) as compared to $\phi < 0°$ ($\phi > 0°$). This suggests that motion of either of the terminal phenyl rings is not symmetric. However, taken together, they are symmetric. Thus, a technique such as X-ray diffraction, which cannot distinguish between two phenyl rings, will find the motion symmetric.

Figure 10 shows the $u(\phi)$ as a function of ϕ, where ϕ is either ϕ_1 or ϕ_2. Here $u(\phi)$ is the average potential experienced by the ring as it executes torsional motion about the long molecular axis. This has been obtained from the probability density function,

$$f(\phi) = C_1 \exp\left(\frac{-u(\phi)}{kT}\right) \tag{10}$$

by inversion. The dihedral angle distributions, $f(\phi)$, can be calculated from the simulations; $u(\phi)$ can be obtained by inversion of eq 10. $u(\phi)$ in Figure 10 at different pressures shows that the functional dependence of the potential energy of two neighboring rings on the torsional angle ϕ (ϕ_1 or ϕ_2) is seen to alter drastically with pressure. It transforms from W-shaped to U-shaped as a function of pressure. This behavior is in excellent agreement with the Raman scattering studies by Guha et al.[4,5] They studied polyphenyls such as biphenyl and *p*-hexaphenyl.

Generally, increasing the temperature does not change the actual shape of the potential energy curve but promotes the molecules to a higher energy state. But the pressure variation alters the form of the potential energy curve itself. Note that the transformation from W-shaped to U-shaped potential occurs in the pressure range 1.0−1.5 GPa. The $\Delta E_{\text{np}\rightarrow\text{p}}$ (the energy difference between the nonplanar (np) state and planar state (p)) is calculated at various pressures from Figure 10. These are listed in Table 6. Table 6 also shows the percentage population of nonplanar molecules (*n*) at various pressures. These are plotted in Figure 11 along with a fit to the polynomial $n = a_0 + a_1P + a_2P^2$ (where *P* stands for pressure). We found that a_0, a_1, and a_2 are 71.8238, −90.9246, and 28.2591, respectively. By interpolation we find $P = 1.394$ GPa at $n = 0$. In other words, the transformation from the disordered phase to the ordered phase in which the molecules are completely planar occurs at $P = 1.394$ GPa. Here, we have considered all the molecules within $\phi = \pm 25°$ as planar. The reason for this choice arises

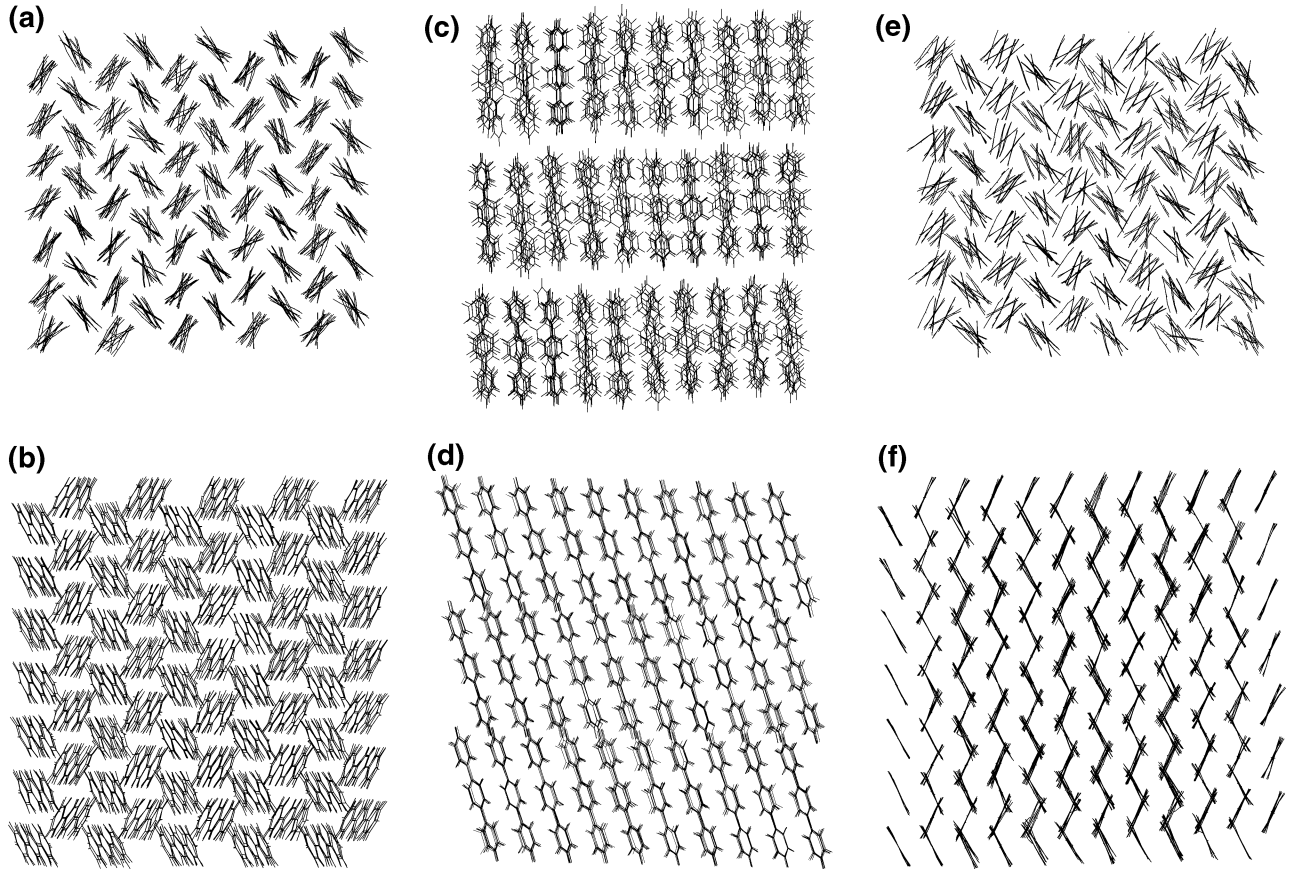

Figure 6. The snapshots of molecules: along the *c*-axis at (a) 1 atm and 300 K and(b) 5.0 GPa and 300 K; along the *b*-axis at (c) 1 atm and 300 K and (d) 5.0 GPa and 300 K; along long molecular axis at (e) 1 atm and 300 K and (f) 5.0 GPa and 300 K.

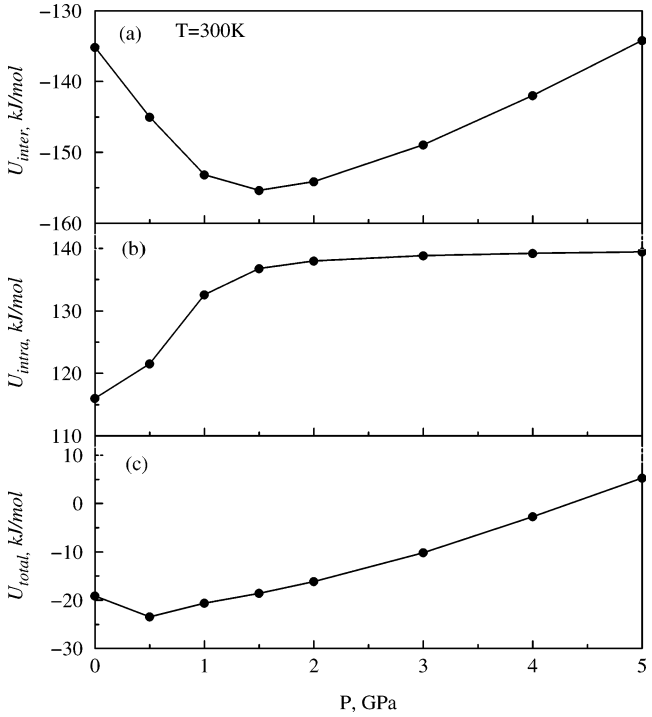

Figure 7. Variation of (a) intermolecular energy, (b) intramolecular energy, and (c) total interaction energy as a function of pressure.

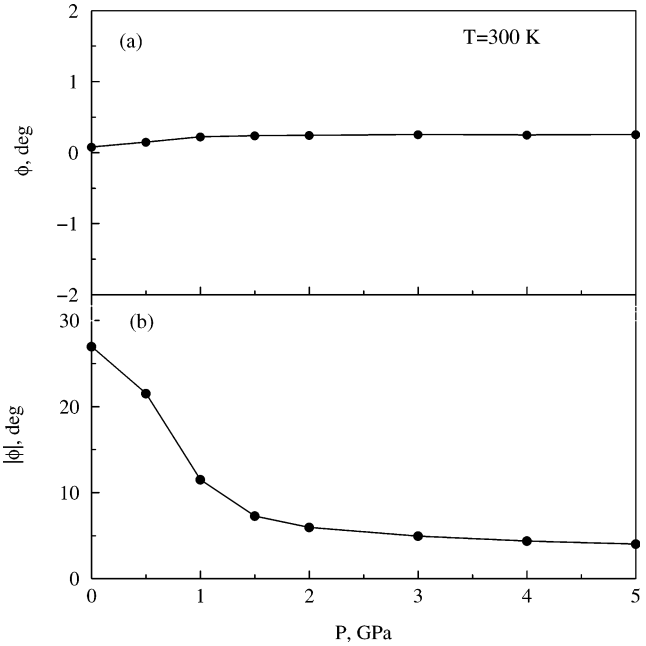

Figure 8. Average (a) dihedral angle and (b) absolute dihedral angle as a function of pressure.

from the fact that $f(\phi)$ has a full width half-maximum of $\phi = \pm 25°$ at 1.5 GPa by which pressure complete planarity has been achieved.

Figure 12 shows the contour plots of the probability density of ϕ_1 and ϕ_2 over the pressure range from 1 atm to 5 GPa. This has been obtained from the instantaneous values of ϕ_1 and ϕ_2 averaged over all the molecules and MC steps at different pressures. From the figure it is clear that $\phi_1 = -\phi_2$ at all the pressures. This suggests that the molecule is on the average performing torsional motions preserving centrosymmetry. The contour plots are consistent with the change from W-potential to U-potential at higher pressures.

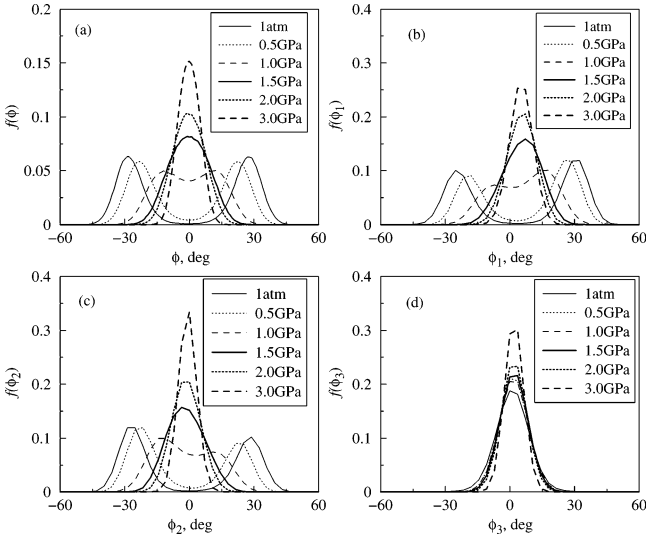

Figure 9. Average dihedral angle distributions (a) $f(\phi)$ averaged over both the dihedral angles ϕ_1 and ϕ_2, (b) $f(\phi_1)$, (c) $f(\phi_2)$, and (d) $f(\phi_3)$.

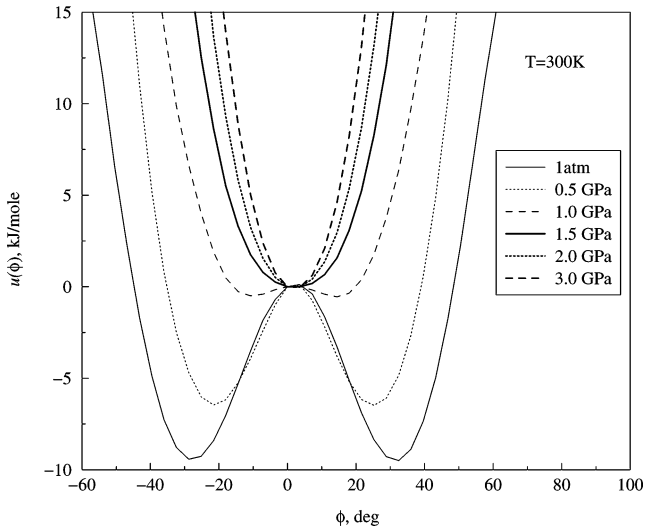

Figure 10. $U_{total}(\phi)$ as a function of pressure at 300 K.

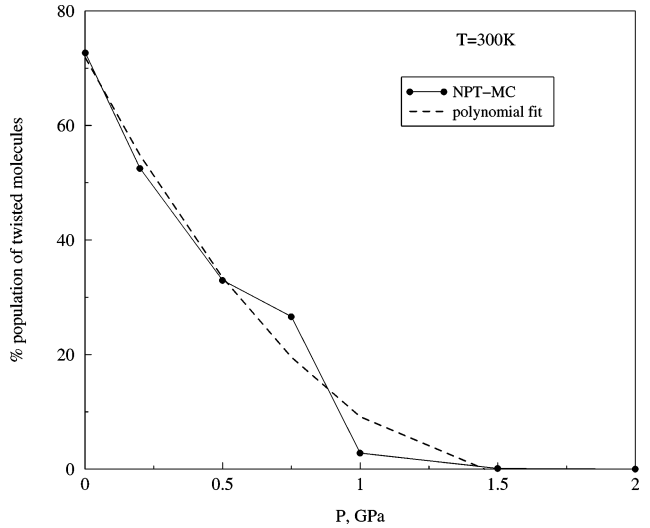

Figure 11. The percentage population of twisted molecules as a function of pressure with a polynomial fit.

Figure 13 shows the variation of the quantities $\langle u_x^2 \rangle$, $\langle u_y^2 \rangle$, and $\langle u_z^2 \rangle$ (mean square displacement along *x*, *y*, and *z* direction for atoms) as a function of pressure for a few of the atoms.

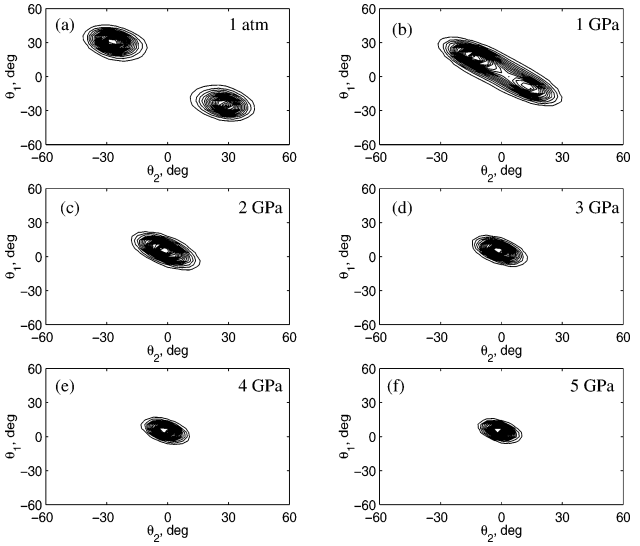

Figure 12. Contour plot of joint probability density $f(\phi_1,\phi_2)$ of instantaneous inter-ring torsions ϕ_1 and ϕ_2 at 300 K and (a) at 1 atm, (b) 1.0 GPa, (c) 2.0 GPa, (d) 3.0 GPa, (e) 4.0 GPa, and (f) 5.0 GPa.

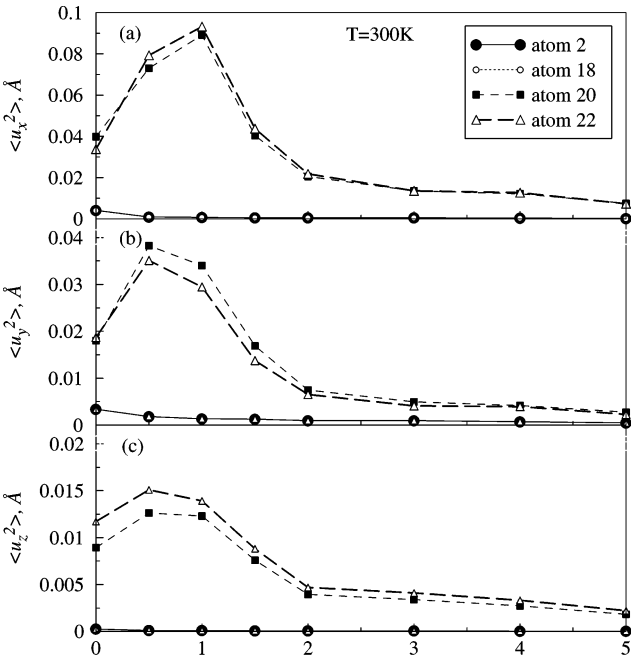

Figure 13. Quantities u_x^2, u_y^2, and u_z^2 as a function of pressure for atoms 2, 18, 20, and 22 (see Figure 1) in the (a) *x*-, (b) *y*-, and (c) *z*-direction.

TABLE 6: $\Delta E_{np \rightarrow p}$ as a Function of Pressure at 300 K and Percentage Population of Nonplanar (Twisted) Molecules

P, GPa	$\Delta E_{np \rightarrow p}$, kJ/mol	percentage population of nonplanar molecules
0.000 1	9.43	72.66
0.200 0	8.94	52.48
0.500 0	6.43	32.95
0.750 0	5.14	26.64
1.000 0	0.49	2.80

Atoms chosen are para carbon atoms of the central ring and H atoms at ortho positions of the central ring. The former lie on the molecular axis, while the latter lie away from the axis. These, therefore, give an indication of the displacements originating purely as a result of torsional motions. The quantities are calculated from

$$\langle u_\alpha{}^2 \rangle = \langle (\bar{\alpha} - \alpha)^2 \rangle_{N,l} \quad (11)$$

where $\alpha = x, y, z$. $\langle\ \rangle_{N,l}$ indicates an average over all particles (N) and simulation steps (l). $u_x{}^2$, $u_y{}^2$, and $u_z{}^2$ are close to $u_a{}^2$, $u_b{}^2$, and $u_c{}^2$ (which are the displacements along the cell vectors) since angles α, β, and γ are nearly orthogonal. It is evident that the amplitude of displacement of the atoms at the para positions are significantly lower than those at ortho positions. Also, note that $u_x{}^2$ is approximately 2 times greater than $u_y{}^2$ which is approximately 2 times greater than $u_z{}^2$ showing that the amplitude of librations is significant along x- and y-directions. Another interesting observation that can be made is that the displacement $\langle u_x{}^2 \rangle$ exhibits a maximum near the transition pressure. This maximum in $\langle u_x{}^2 \rangle$ near the transition pressure arises from two factors. First, the change from W- to U-potential is associated with a change from the saddle point (potential maximum) to a potential minimum at $\phi = 0°$. This leads to a significant increase in the populations around $\phi = 0°$. Further, a relatively flat U-potential at $\phi = 0°$ permits an increase in displacement: at low pressures, fewer molecules were performing the large amplitude motion ($\phi = -30°$ to $30°$, see Figure 9). But this motion was infrequent as a result of a barrier at $\phi = 0°$ (see Figure 10). At $P = 1.0$ GPa, the potential is relatively flat with little or no barrier at $\phi = 0°$ (see dashed curve in Figure 10). By 1.5 GPa, the U-potential has a large curvature (second derivative) at $\phi = 0°$ which leads to reduced freedom and restricted torsional motion. This leads to a decrease in the amplitude of $\langle u_x{}^2 \rangle$ and $\langle u_y{}^2 \rangle$.

5. Conclusions

p-Terphenyl at 300 K and 1 atm pressure has been studied using four different sets of intermolecular and intramolecular potentials. The set of Filippini's modified intermolecular interactions and BHS intramolecular potential provides the best description of the structure.

The present study suggests that *p*-terphenyl transforms to an ordered phase around 1.4 GPa. This has been estimated from the polynomial fit to $n(P)$, the pressure dependence of the percentage population of nonplanar molecules. This transformation is accompanied by a change in the functional form of the potential energy curve associated with inter-ring flipping from W-shape to U-shape. This is in excellent agreement with the previous high-pressure Raman studies of Guha et al.[4,5] They found that polyphenyls such as *p*-hexaphenyl also show a transformation to an ordered planar conformation, an increase in pressure, and that this transformation is accompanied by change from W-shape to U-shape in the potential energy curve. We find no discontinuities in volume or intermolecular interaction energy with increase in pressure. Interestingly, we find the amplitude of the torsional motion is largest around 1.0 GPa. This can be attributed to the relatively flat potential energy curve $u(\phi)$ near $\phi = 0°$.

Acknowledgment. N.A.M. and S.Y. thank the Department of Science & Technology, New Delhi and BRNS, DAE, Mumbai for financial support.

References and Notes

(1) Baudour, J. L.; Delugeard, Y.; Cailleau, H. *Acta Crystallogr.* **1976**, *B32*, 150.
(2) Baudour, J. L.; Cailleau, H. *Acta Crystallogr.* **1977**, *B33*, 1773.
(3) Cailleau, H.; Baudour, J. L.; Zoyen, C. M. *Acta Crystallogr.* **1979**, *B35*, 426.
(4) Guha, S.; Graupner, W.; Resel, R.; Chandrasekhar, M.; Chandrasekhar, H. R.; Glaser, R.; Leising, G. *J. Phys. Chem.* **2001**, *A105*, 6203.
(5) Guha, S.; Graupner, W.; Resel, R.; Chandrasekhar, M.; Chandrasekhar, H. R.; Glaser, R.; Leising, G. *Phys. Rev. Lett.* **1999**, *82*, 3625.
(6) Heimel, G.; Puschnig, P.; Oehzelt, M.; Hummer, K.; Koppelhuber-Bitschnau, B.; Porsch, F.; Ambrosch-Draxl, C.; Resel, R. *J. Phys: Condens. Matter* **2003**, *15*, 3375.
(7) Puschnig, P.; Heimel, G.; Weinmeier, K.; Resel, R.; Ambrosch-Draxl, C. *High Pressure Res.* **2002**, *22*, 105.
(8) Baranyai, A.; Welberry, T. R. *Mol. Phys.* **1992**, *75*, 867.
(9) Bordat, P.; Brown, R. *Chem. Phys.* **1999**, *246*, 323.
(10) Tsuzuki, S.; Tanabe, K. *J. Phys. Chem.* **1991**, *95*, 139.
(11) Williams, D. E.; Cox, S. R. *Acta Crystallogr.* **1984**, *B40*, 404.
(12) Filippini, G.; Gavezzotti, A. *Acta Crystallogr.* **1993**, *B49*, 868.
(13) Williams, D. E. *J. Chem. Phys.* **1967**, *47*, 4680.
(14) Baudour, J. L.; Delugeard, Y.; Cailleau, H. *Acta Crystallogr.* **1976**, *B32*, 150.
(15) Benkert, C.; Heine, V.; Simmons, E. H. *J. Phys. Chem.* **1987**, *20*, 3337.
(16) Parrinello, M.; Rahman, A. *Phys. Rev. Lett.* **1980**, *45*, 1196.
(17) Metropolis, N.; Rosenbluth, A. W.; Rosenbluth, M. N.; Teller, A. H.; Teller, E. *J. Chem. Phys.* **1953**, *21*, 1087.
(18) Yashonath, S.; Rao, C. N. R. *Chem. Phys. Lett.* **1985**, *119*, 22.
(19) Martyna, G. J.; Tobias, D. J.; Klein, M. L. *J. Chem. Phys.* **1994**, *101*, 4177.
(20) Murugan, N. A.; Jha, P. C.; Yashonath, S.; Ramasesha, S. *J. Phys. Chem.* **2004**, *B108*, 4178.
(21) Baudour, J. L.; Toupet, L.; Delugeard, Y.; Ghemid, S. *Acta Crystallogr.* **1986**, *C42*, 1211.
(22) Hsu, L. L.; Williams, D. E. *Acta Crystallogr.* **1980**, *A36*, 277.